A major purpose of the Technical Information Center is to provide the broadest dissemination possible of information contained in DOE's Research and Development Reports to business, industry, the academic community, and federal, state and local governments.

Although a small portion of this report is not reproducible, it is being made available to expedite the availability of information on the research discussed herein.

Los Alamos National Laboratory is operated by the University of California for the United States Department of Energy under contract W-7405-ENG-36

LA-UR--84-2555

DE84 016476

TITLE: SIMULATION OF THE INTERACTION OF SINGLE-PULSED OPTICAL LASERS WITH TARGETS IN A VACUUM

MASTER

AUTHOR(S): S. R. Goldman, X-1
G. H. Canavan, P-DO
R. S. Dingus, NSP-SDR
M. A. Mahaffy, X-7

SUBMITTED TO. Fifth International Symposium on Gas Flow and Chemical Lasers
August 20-24, 1984

DISCLAIMER

Los Alamos National Laboratory
Los Alamos, New Mexico 87545

Simulation of the Interaction of Single-Pulsed Optical Lasers with Targets in a Vacuum

S. R. Goldman, G. H. Canavan, R. S. Dingus, and M. A. Mahaffy

Los Alamos National Laboratory, Los Alamos, New Mexico 87545

We present computer simulations of the interaction of a perturbed laser beam on an aluminum target at pulse widths from .05 to 2.0 μsec, and intensities from 5×10^7 to 10^{13} W/cm^2, at laser wavelengths varying from 0.25 μm (KrF laser) to 10.6 μm (CO_2 laser). We focus on impulse coupling, identify the critical processes for momentum generation, and discuss the uncertainties in modeling.

1. Introduction

We have studied a variety of problems for the interaction of perturbed laser beams with aluminum targets at fluences from 10^2 to 10^7 joule/cm^2, pulse widths from .05 to 2.0 μsec, and intensities from 5×10^7 to 10^{13} W/cm^2, at laser wavelengths varying from 0.25 μm (KrF laser) to 10.6 μm (CO_2 laser).

Calculations, using LASNEX, a radiation, plasma-hydrodynamics code, have typically involved inverse bremsstrahlung absorption of the incident laser beam. A fraction of the energy reaching the critical density is partitioned into either suprathermal electrons or a single electron bin. Radiation energy is transported through multigroup diffusion, and electron energy through a combination of Spitzer thermal conductivity and a metal model. Pressure and energy equation of state information is gotten through tables, internal local thermodynamic equilibrium (LTE) calculations, or non-LTE, average atom, rate equations as appropriate. The non-LTE option is typically used at electron temperatures above 20 ev. Opacities are obtained either from tables in the cold opacity limit or from weighting excited state cross sections with the internally calculated electron distribution.

The results below focus on impulse coupling, identify the critical processes for momentum generation, and discuss the uncertainties in modeling.

2. Results for one-dimensional geometry

Figure 1 shows calculations of momentum coupling per incident energy vs fluence Φ, for CO_2 and KrF lasers for 1.0 μsec pulses, over a fluence range from 10^3 to 10^7 J/cm^2 in planar geometry. Experimental points for XeCl (.31 μm) provided by R. Hunter (1984), the higher value, and CO_2 (10.6 μm) provided by King and Phipps (1984), are shown, indicating reasonable agreement for both at the kJ/cm^2 level. Note that below a fluence of 3×10^5 J/cm^2, the coupling, I/E, for KrF varies as $\Phi^{-.42}$, midway between the x-ray coupling result of $\Phi^{-.5}$ and the prediction from simple critical density scaling of $\Phi^{-.33}$ as referred to by G. McCall

(1983). Also interesting is the fact that the KrF and CO_2 curves draw closer at about the MJ/cm^2 level. Multiple entries at the same fluence indicate limits from the usage of differing physical models.

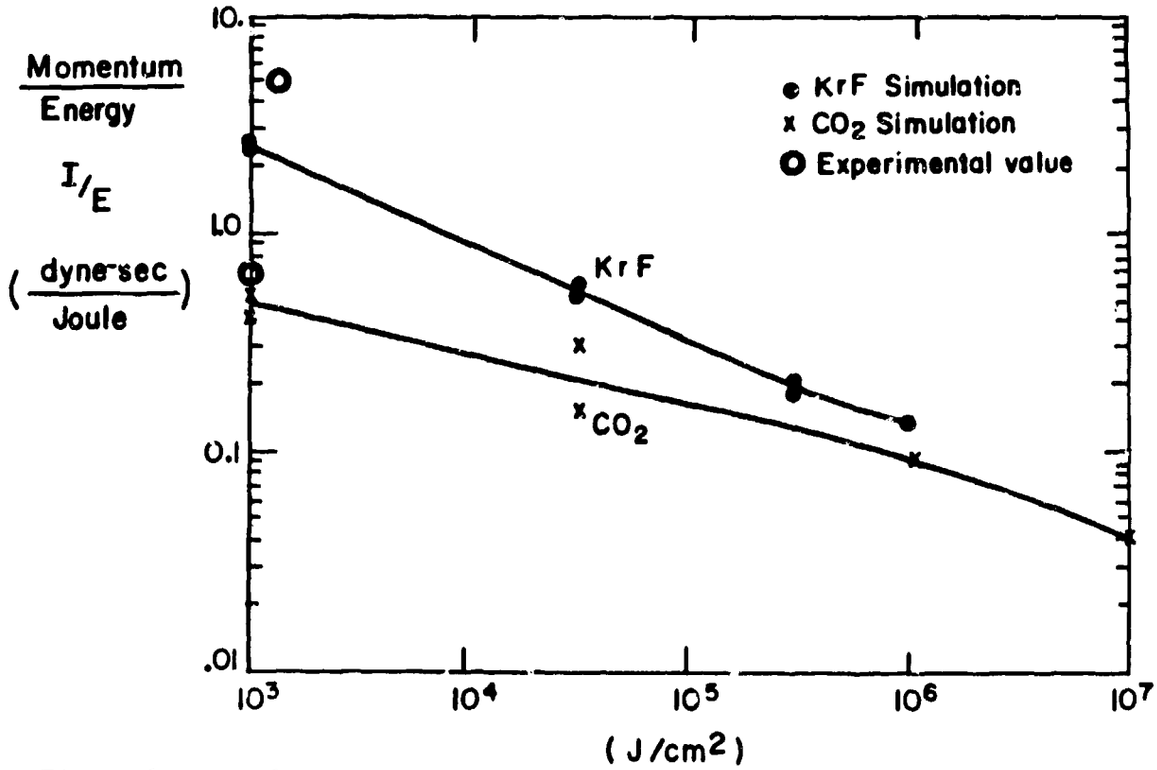

Figure 1. Impulse coupling efficiency as a function of fluence for microsecond pulse lengths.

The decrease in efficiency with increasing fluence and intensity is due primarily to the higher temperature of the blow-off plasma which results in a lower ratio of momentum to energy for the blow-off material.

One factor in the near merging of the KrF and CO_2 curves at higher fluences is increasing radiation emission at higher fluences (and intensities) for the KrF case, at the same time that the radiation emission for the CO_2 is limited by non-equilibrium effects. The fraction of absorbed energy lost as thermal re-radiation is unavailable for momentum. At a fluence of 10^3 J/cm^2, the momentum coupling efficiency of KrF is about 4 to 5 times greater than that for CO_2; at a fluence of 10^6 J/cm^2 the ratio of KrF to CO_2 efficiency is of order 1.5. Over the fluence range from 10^3-10^6 J/cm^2, the ratio of vaporized masses containing 90% of the outwardly directed momentum is about 3/1. Hence the ratio of ablated mass for KrF and CO_2 at the same fluence is roughly constant. On the other hand, for KrF the re-radiation loss fraction goes from 0.2 at 10^3 J/cm^2 to 0.75 at 3 x 10^4 J/cm^2 to 0.79 at 10^6 J/cm^2, while for CO_2 the same fraction goes from 0.5 at 10^3 J/cm^2 to 0.7 at 3 x 10^4 J/cm^2 to 0.3 at 10^6 J/cm^2 and 0.24 at 10^7 J/cm^2. For CO_2, the plasma temperature becomes high enough that the radiation losses are suppressed by non-equilibrium effects while for KrF, due to its lower coronal temperatures and higher densities, the dominant effect is the rise in temperature and hence an increase in re-radiation loss without non-equilibrium limitation.

Other effects must also be present. The KrF curve is virtually a straight line from 10^3 to 3×10^5 J/cm^2 even though the increase in re-radiated energy is almost entirely between 10^3 and 3×10^3 and 3×10^4 J/cm^2.

Rather than seeking correlation between KrF and CO_2 at a given fluence, it is more profitable to compare calculations at a similar I/E. Figure 2 shows the temperature profiles for a KrF fluence of 10^6 J/cm^2 and a CO_2 fluence of 3×10^4 J/cm^2, which by Fig. 1 have about the same coupling coefficient. The material and radiation temperatures have similar values and variations in the corona. The profiles outside the ablation surface are simply compressed for CO_2 relative to KrF. This is consistent with deposition in more dense material by the shorter wavelength radiation as well as the greater fluence.

At fixed intensity, momentum coupling is stronger for shorter pulses. This is presumably due to less shielding of the target from the incident laser beam by the less extended corona. For pulses of length 5×10^{-8} sec instead of 10^{-6} sec for KrF the value of I/E increases by a factor of 2 to 2.5 over the intensity range from 2×10^{10} to 6×10^{11} W/cm^2; for CO_2 over the same intensity range, I/E increases by a factor of 1.5.

Among the physical factors controlling momentum production are the laser absorption processes, the spectrum of electrons produced through absorption, radiation emission from the target to the vacuum, radiation transport from the absorption region into the target, and electron thermal conductivity. At low intensities, where there are prominent regions at temperatures on the order of 1 ev and densities below normal, the effective free electron density, and the models for transport behavior are uncertain. At higher intensities and temperatures, the non-LTE modeling is in question.

In Fig. 1, limits (multiple crosses) for CO_2 at 10^3 J/cm^2 (about 25% variation) are due to the difference between using a cold opacity model for aluminum below temperatures of 10 ev (upper value) and using an opacity model calculated for electrons in Saha equilibrium. The limits

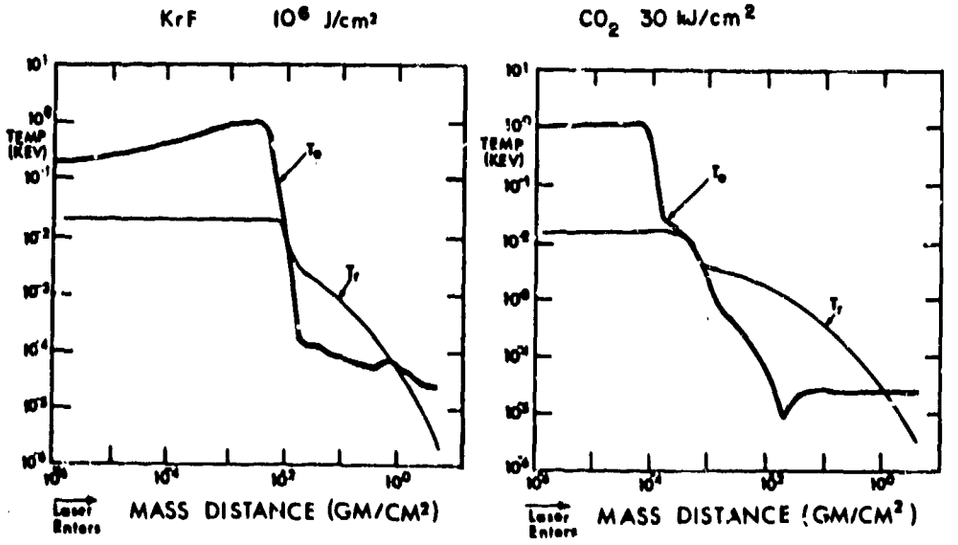

Figure 2. Temperature profiles as functions of mass distance from target on right. Laser beams incident from left (1 μs pulse)

for CO_2 at 3×10^4 J/cm^2 (about a factor of two apart) are due to turning on the non-LTE rate equations at 40 ev (lower value) and 10 ev, and using a Saha equilibrium at temperatures below.

The limits for KrF at all fluences (multiple dots) differed by less than 15%. The following forms of variation were tested with fluences and differences indicated in order in parentheses:

a) laser absorption at critical density into suprathermals or a single temperature background (10^3, 3×10^4; < 5%)
b) electrons treated by LTE or non-LTE above 10 ev (10^3, 3×10^4, 3×10^5; < 15%)
c) opacity variation by a factor of 10 around nominal (10^3; < 5%)
d) opacity variation between a cold opacity and Saha based opacity below 10 ev (10^3, 3×10^4; < 7%)
e) electron heat flow limited by $.03\, v_e n_e T_e$ or $1.0\, v_e n_e T_e$, with v_e, n_e and T_e respectively electron thermal velocity, electron density and electron temperature (10^3; < 4%)
f) electron heat flow modeled after metal at low temperatures or solely plasma (10^3; <4%)

The heat flow into the solid target for the metal model was ten to one hundred times greater than with the plasma model, but the effect on ablation was not significant.

At all fluences presented in Fig. 1 for both CO_2 and KrF, the fraction of total energy deposited into suprathermals to vaporize the initial solid was less than 1%; hence the details of the solid absorption process were not felt to be important.

3. Results for spherically symmetric geometry

We have also done calculations appropriate to a single-pulsed XeF excimer laser (λ = 0.35 μm) with a pulse length of 2.0 μsec using both planar and spherical ("1.5-dimensional") models. The latter option allows the expansion to fan out in order to simulate the expansion from a finite spot. For an angle of 11^o the area increases by a factor of 2 at a distance out from the original target surface equal to the laser spot diameter. In simulations of spherical geometry by means of a sector of a sphere, momentum is not conserved exactly because of divergence effects in the fluid flow involving the pressure. Outwardly directed momentum is artificially increased and inwardly directed momentum is artificially decreased. Hence a lower bound, the open circles, on the directed momentum is gotten by using the inwardly directed momentum, and an averaged estimate, the crosses, is gotten by using the average of the magnitudes of the inwardly and outwardly directed momenta.

The momentum coupling efficiency from the calculations is shown in Fig. 3. The lower bound results and the flat results (closed circles) are essentially the same over the fluence range 10^2 - 10^3 J/cm^2. The averaged estimate is of the order of 35% higher at the peak experimental fluences. The correction is in the direction required to bring theory up to the values of the kJ/cm^2 experiments in Figure 1, suggesting that the experimental results contain 2-d effects. The increase in momentum coupling for the spherical runs is understandable in terms of greater mass ablation (shown in Fig. 4) and lower re-radiation loss. With spherical divergence to penetration the laser light penetrates deeper into the target primarily due to a decrease in the blow-off plasma scale-length. The coronal plasma temperature is lowered; this raises the opacity, and decreases losses

through re-radiation. Profiles of comparative electron temperatures (T_e, ion temperatures (T_i, and radiation temperatures (T_r) are shown in Figure 5. Note the significantly lower radiation temperature for the spherical case.

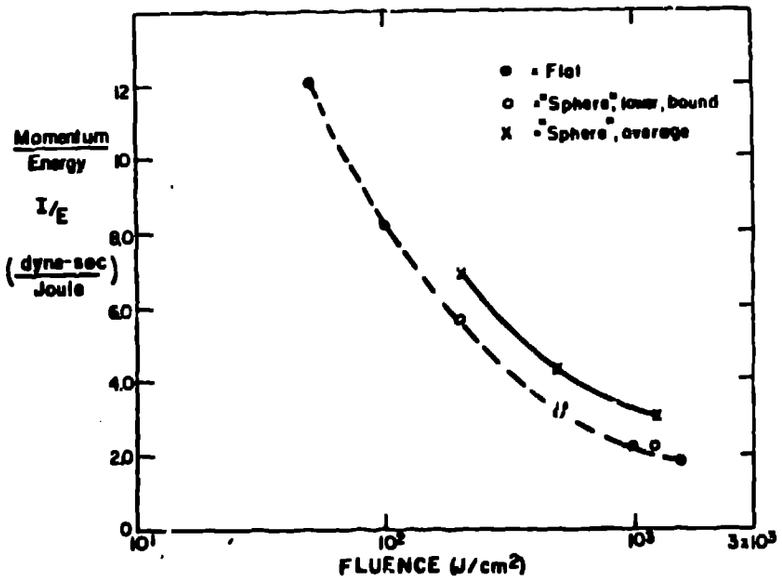

Figure 3. Momentum conversion efficiency for XeF laser (λ = 0.35 μm) on aluminum (flat and spherical geometry)

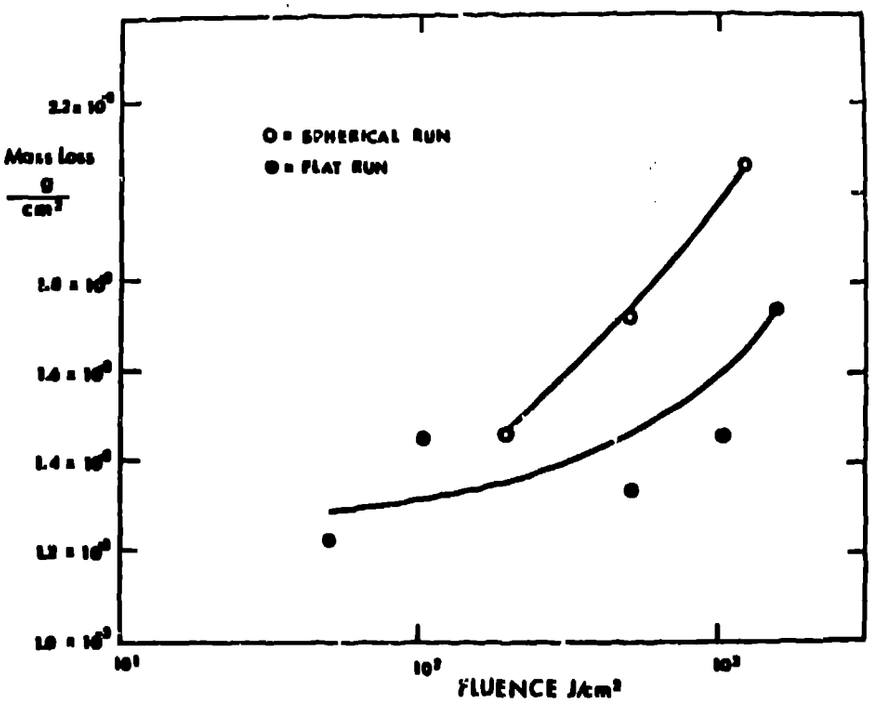

Figure 4. Mass loss as a function of fluence for XeF laser on aluminum (flat and spherical geometry)

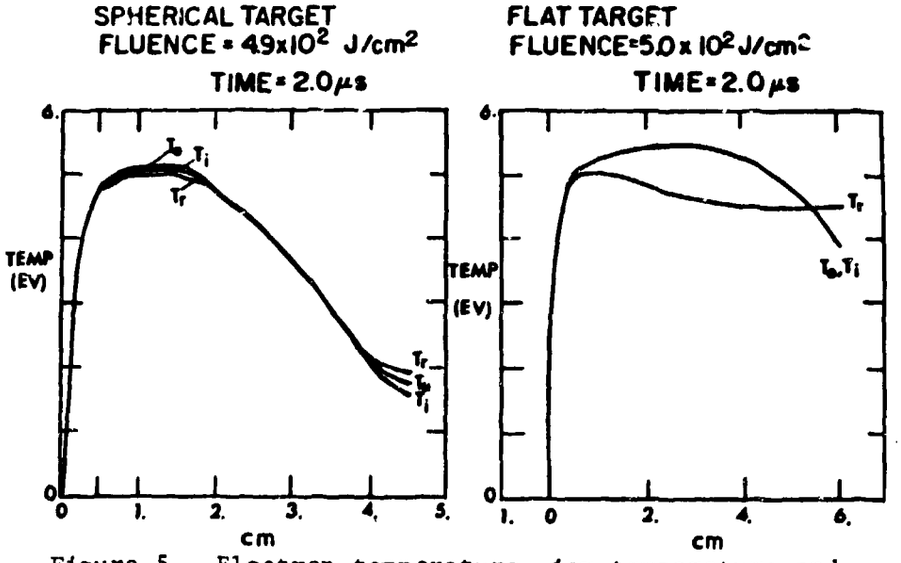

Figure 5. Electron temperature, ion temperature and radiation temperature (T_e, T_i, T_r) as functions of position at end of pulse for XeF on Al, flat and spherical geometry.

Conclusions

For non-diverging flow, at the KrF laser wavelength (.265 μm) we obtain a momentum coupling efficiency (I/E; I = impulse, E = pulse energy) scaling roughly with the fluence Φ as $\Phi^{-.42}$, with detailed variation indicated on Fig. 1, in the fluence range from 10^3 to 10^6 J/cm^2 for micro-second pulses. Changes in I/E are less than 15% over a range of physical modeling variations.

The scaling of momentum coupling with fluence is less exact at 10.6 μm laser wavelength (CO_2) since the calculations are more sensitive to modeling variations, in particular to temperature at which non-LTE physics is turned on. The coupling efficiency is always lower at the longer wavelength but it decreases less rapidly with increasing fluence. This appears to be largely attributable to a differing re-radiation loss variation with fluence.

For both wavelengths efficiencies are higher at shorter pulse length and the same intensity. This is due to less shielding of the solid target from the incident laser with less material.

The variation due to diverging flow is significant even at the lower range of intensities and fluence because of the greater mass ablation and laser penetration into the target material which accompanies the sharper density gradients. It is expected that this effect will be even greater for experimentally obtainable conditions with small laser spot size compared to coronal length. The sensitivity can be investigated through two-dimensional simulations.

This work was sponsored in part by the U. S. Department of Energy and in part by the Air Force Weapons Laboratory.

Hunter, R. 1984 private communication
King, T. R. and Phipps, C. R. 1984 private communication
McCall, G. 1983 Plasma Physics 25 237